J|A|C|S
ARTICLES
Published on Web 08/28/2004

Multielectron Photoreduction of a Bridged Ruthenium Dimer, $[(phen)_2Ru(tatpp)Ru(phen)_2][PF_6]_4$: Aqueous Reactivity and Chemical and Spectroelectrochemical Identification of the Photoproducts

Rama Konduri, Norma R. de Tacconi, Krishnan Rajeshwar, and Frederick M. MacDonnell*

Contribution from the Department of Chemistry and Biochemistry, The University of Texas at Arlington, 502 Yates Street, Arlington, Texas 76019

Received April 9, 2004; E-mail: macdonn@uta.edu

Abstract: The dinuclear ruthenium(II) complex $[(phen)_2Ru(tatpp)Ru(phen)_2][PF_6]_4$ (**P**) (where phen is 1,10-phenanthroline and tatpp is 9,11,20,22-tetraazatetrapyrido[3,2-*a*:2′3′-*c*:3″,2″-*l*:2‴,3‴]pentacene) is shown to accept up to four electrons and two protons on the central tatpp bridging ligand via a combination of stoichiometric chemical reductions and protonations and spectroelectrochemistry (SEC) in acetonitrile. The absorption spectra of seven distinct species related by reduction and/or protonation of the central tatpp ligand were obtained and the two sequential photoproducts obtained from visible irradiation of **P** in acetonitrile (with 0.25 M triethylamine (TEA)) thus identified as $\mathbf{P}^-$ (singly reduced, nonprotonated **P**) and $\mathbf{HP}^-$ (doubly reduced, monoprotonated **P**), respectively. Importantly, the photochemical activity is maintained in mixed water−acetonitrile (1:4) solutions under basic conditions, and the protonation state of the photoproducts is readily controlled by varying the solution pH between 8 and 12. Absorption spectra obtained by SEC under similar solvent conditions were virtually identical to those obtained photochemically, and thus the doubly reduced photoproducts were identified as $\mathbf{P}^{2-}$ (pH 12), $\mathbf{HP}^-$ (pH 10), and $\mathbf{H_2P}$ (pH 8). This last photoproduct, $\mathbf{H_2P}$, is particularly promising with respect to solar hydrogen production in that it can be produced in the presence of water and its dehydrogenation under appropriate conditions could yield H_2 and regenerate **P**. A qualitative MO diagram is presented as a framework for understanding the observed optical transitions as a function of oxidation and protonation state.

Introduction

Ruthenium−polypyridyl complexes are one of the most widely studied chromophores for molecular light-to-chemical energy conversion because of their favorable photophysical properties and chemical stability.[1,2] A huge variety of monomeric, oligomeric, dendrimeric, and polymeric assemblies of the $[Ru(bpy)_3]^{2+}$ complex or closely related complexes have been prepared and, in many cases, shown to efficiently capture and collect light energy.[1,3−7] This has clear relevance to solar energy conversion schemes. However, nearly all such assemblies are limited to driving one-electron processes.[8] On the other hand, important practical reactions such as dioxygen reduction and hydrogen generation require concerted multielectron transfer.

Aside from polymeric assemblies,[9] Brewer and co-workers were first to demonstrate that a single supramolecular assembly, comprised of a Ru−Ir−Ru polypyridyl triad, could store two electrons on the two polyazine bridging ligands within its structure upon photoirradiation in the presence of a sacrifical donor.[10] Substitution of Rh(III) for the Ir(III) resulted in a Ru−Rh−Ru assembly in which the photoreduction is centered at the Rh(III) site, leading to the possibility of catalysis using a Rh(III/I) couple.[11,12]

Recently, we reported that the dinuclear Ru(II) complexes **P** and **Q** (Figure 1) were capable of reversibly storing a maximum of two or four electrons, respectively, upon visible light irradiation in acetonitrile and in the presence of sacrificial reductant agents.[13] In both complexes, it was proposed that the central part of the bridging ligand plays both the role of the electron acceptor subunit for the photoinduced charge-separation process and the role of the multielectron storage unit. Reduction

(1) Balzani, V.; Juris, A.; Venturi, M.; Campagna, S.; Serroni, S. *Chem. Rev.* **1996**, *96*, 759−833.
(2) Kalyanasundararam, K. *Photochemistry of Polypyridine and Porphyrin Complexes*; Academic Press: London, 1992.
(3) Balzani, V.; Scandola, F. *Supramolecular Photochemistry*; Horwood: Chichester, U.K., 1991.
(4) Balzani, V.; Ceroni, P.; Maestri, M.; Saudan, C.; Vicinelli, V. *Top. Curr. Chem.* **2003**, *228*, 159−191.
(5) Balzani, V.; Campagna, S.; Denti, G.; Juris, A.; Serroni, S.; Venturi, M. *Acc. Chem. Res.* **1998**, *31*, 26−34.
(6) Baxter, S. M.; Jones, W. E., Jr.; Danielson, E.; Worl, L. A.; Strouse, G. F.; Younathan, J. N.; Meyer, T. J. *Coord. Chem. Rev.* **1991**, *111*, 47−71.
(7) Dupray, L. M.; Devenney, M.; Striplin, D. R.; Meyer, T. J. *J. Am. Chem. Soc.* **1997**, *119*, 10243−10244.
(8) Watts, R. J. *Comm. Inorg. Chem.* **1991**, *11*, 303−337.
(9) Worl, L. A.; Strouse, G. F.; Younathan, J. N.; Baxter, S. M.; Meyer, T. J. *J. Am. Chem. Soc.* **1990**, *112*, 7571−7578.
(10) Molnar, S. M.; Nallas, G.; Bridgewater, J. S.; Brewer, K. J. *J. Am. Chem. Soc.* **1994**, *116*, 5206−5210.
(11) Swavey, S.; Brewer, K. J. *Inorg. Chem.* **2002**, *41*, 4044−4050.
(12) Holder, A. A.; Swavey, S.; Brewer, K. J. *Inorg. Chem.* **2004**, *43*, 303−308.
(13) Konduri, R.; Ye, H.; MacDonnell, F. M.; Serroni, S.; Campagna, S.; Rajeshwar, K. *Angew. Chem., Int. Ed.* **2002**, *41*, 3815−3187.

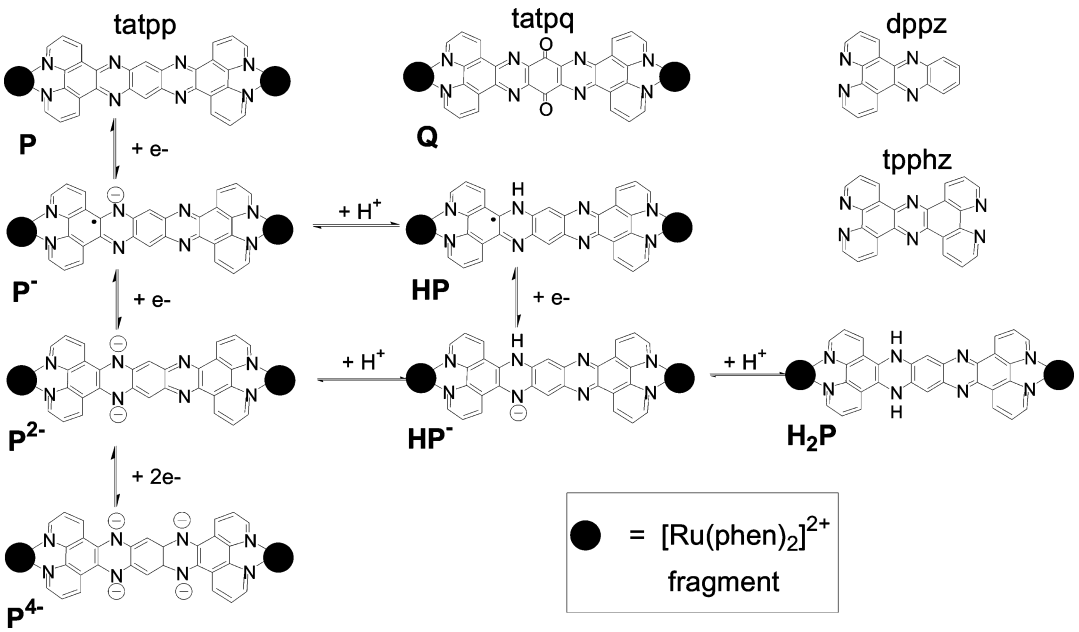

Figure 1. Structural drawing of the complexes **P** and **Q** and the related redox and protonation isomers for **P**. The structures of the related DPPZ and TPPHZ ligands are also shown.

of the tatpp bridging ligand in **P** was observed directly using transient absorption spectroscopy and, remarkably, showed that the charge-separated intermediate had a lifetime of 1.3 μs in dichloromethane.[14]

Here we report on the reduction behavior of **P**. Importantly, we show that the photochemical ability of **P** to undergo two sequential one-electron reductions (to form the singly reduced $\mathbf{P}^{-}$ and the doubly reduced $\mathbf{P}^{2-}$) is maintained in mixed water−acetonitrile solutions under basic conditions. The photochemical activity of **P** in aqueous media considerably expands its potential use toward a number of important substrates, including water, and its environmental adaptability. The absorption spectra of the two reduced species, $\mathbf{P}^{-}$ and $\mathbf{P}^{2-}$, were found to depend on the solution pH, indicative of protonation(s) at the central reduced sites. To determine the identity of these solution species, we first undertook an extensive analysis of the absorption spectra of the redox and protonation isomers of **P** as generated by chemical, spectroelectrochemical, and photochemical means in both dry acetonitrile solution and mixed water−acetonitrile solutions. The notation used in Figure 1 will be used to identify these isomers, which are related by one-electron reduction/oxidation vertically and by protonation/deprotonation horizontally. It is important to realize that **P** itself is a large metal complex (over 2 nm long) carrying an overall 4+ charge from the two Ru(II) ions coordinated to the tatpp bridging ligand. We note that many of the isomers can exist in multiple tautomeric forms, and we lack the necessary data to distinguish between them. The tautomers shown reflect our current best guess which is based, in part, on a comparison with the tautomers established for various redox isomers of tetraazapentacene.[15]

Experimental Section

Cobaltocene (Alfa), trifluoroacetic acid (Alfa), and sodium borohydride (Aldrich) were used as received. Acetonitrile (Aldrich, 99.93+%, HPLC grade) was kept over molecular sieves (3 Å) and passed through a column packed with neutral chromatographic alumina just before use. The complex **P** was prepared as described previously.[16] All redox and protonation titrations were carried out in a nitrogen atmosphere glovebox. Stock solutions of **P** (1.09×10^{-4} M), $Co(Cp)_2$ (0.011 M), and trifluoroacetic acid (TFA) (0.013 M) were prepared in thoroughly degassed acetonitrile. $\mathbf{P}^{-}$ and $\mathbf{P}^{2-}$ were generated by adding 1 and 2 equiv of $Co(Cp)_2$, respectively. The protonated isomers were generated by stoichiometric addition of TFA to solutions of $\mathbf{P}^{-}$ and $\mathbf{P}^{2-}$. Reductions with sodium borohydride (0.5 M in diethoxy ether) were done using a 10-fold molar excess of reductant to **P** in 20% water−acetonitrile.

Cyclic voltammetry (CV) and differential pulse voltammetry (DPV) experiments were performed using a PC-controlled potentiostat (CH Instruments, electrochemical analyzer). Either glassy carbon (1.5 mm diameter disk) or Au (1.0 mm diameter disk) working electrodes from Cypress Systems were used. Immediately before use, the electrodes were polished to a mirror finish with wet alumina (Buehler, 0.05 μm), followed by rinsing with Millipore Milli-Q water, dried, and stored in acetonitrile during the preparation of the electrochemical cell. A Pt wire and a premium "no leak" Ag/AgCl reference electrode (Cypress, model EE009) were used as counter and reference electrodes, respectively, and potentials are quoted with respect to this reference. Experiments were conducted in dry acetonitrile (Aldrich, 99.93+%, HPLC grade) with 0.1 M $NBu_4^nPF_6$ (Sigma) as supporting electrolyte, and in 20% water−acetonitrile mixtures at four selected pH values in the range 4−12. In these cases, the aqueous portion contained 0.1 M NaH_2PO_4/0.1 M K_2HPO_4 buffer, and the pH of the water−acetonitrile solution was adjusted with 0.5 M NaOH or 0.5 M H_3PO_4 as measured by a standard glass electrode and pH meter. Prior to each measurement, the solutions were deoxygenated by bubbling with argon, and this atmosphere was maintained over the electrochemical solution throughout the course of the experiment. The cell ohmic resistance was always compensated. All experiments pertain to the laboratory ambient temperature (20 ± 2 °C).

Spectroelectrochemical measurements were performed in transmission mode using a Hewlett-Packard diode array spectrometer (model 8453). A quartz thin-layer cell containing a gold mesh as working

(14) Chiorboli, C.; Fracasso, S.; Scandola, F.; Campagna, S.; Serroni, S.; Konduri, R.; MacDonnell, F. M. *Chem. Commun.* **2003**, 1658−1659.
(15) Sawtschenko, L.; Jobst, K.; Neudeck, A.; Dunsch, L. *Electrochim. Acta* **1996**, *41*, 123−131.
(16) Kim, M.-J.; Konduri, R.; Ye, H.; MacDonnell, F. M.; Puntoriero, F.; Serroni, S.; Campagna, S.; Holder, T.; Kinsel, G.; Rajeshwar, K. *Inorg. Chem.* **2002**, *41*, 2471−2476.

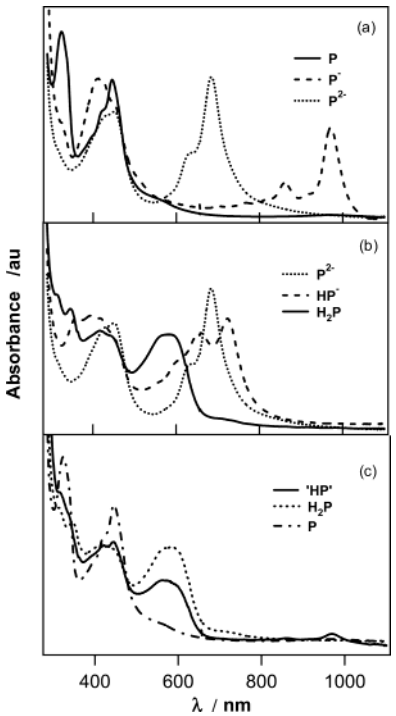

Figure 2. (a) Absorption spectra of **P** (ca. 12 μM, solid line) after addition of 1.0 molar equiv of cobaltocene (dashed line, $\mathbf{P}^-$) and 2.0 molar equiv of cobaltocene (dotted line, $\mathbf{P}^{2-}$) in dry, degassed acetonitrile. (b) Absorption spectra of $\mathbf{P}^{2-}$ (ca. 12 μM, dotted line) after addition of 1.0 molar equiv of TFA (dashed line, $\mathbf{HP}^-$) and 2.0 molar equiv of TFA (solid line, $\mathbf{H_2P}$) in dry, degassed acetonitrile. (c) Absorption spectra of $\mathbf{P}^-$ after addition of 1.0 equiv of TFA (solid line, "**HP**") in dry, degassed acetonitrile. Spectrum of **P** (dashed line) and $\mathbf{H_2P}$ (dotted line) overlaid at same concentration.

electrode[17] was placed inside a 1-cm-path quartz cuvette containing ca. 0.5 mL of **P** solution (2−10 μM). The **P** solution filled the thin-layer space where the gold mesh was located by capillary action.[17] The counter electrode (platinum wire) and the Ag/Ag^+ quasireference electrode were laterally located in the quartz cuvette and next to the capillary slit.

For the photochemical experiments, all solutions were sealed in a quartz or glass cuvette with a rubber septum and degassed for 10 min with nitrogen or argon gas prior to irradiation. Typical solutions were 16 μM in **P** and 0.25 M triethylamine (TEA). The cuvettes were immersed in a water bath (18 ± 2 °C) and irradiated using a 100-W tungsten bulb with a 360-nm-cutoff UV filter. The source-to-sample distance was approximately 3 cm, and the measured photon flux at the sample was 1.125×10^6 lux (as measured by a Lutron LX101 meter). The progress of the photochemical reaction was monitored by periodically removing the cuvette from the water bath and recording the absorption spectra (HP 8453A UV−vis system). For the 20% water−acetonitrile solutions, the pH of the solution was adjusted by adding acetic acid. The solution composition for electrochemical and photochemical reactions in 20% water−acetonitrile could not be made identical due to the requirement for $NBu^n_4PF_6$ in the electrochemical experiments and for TEA in the photochemical experiments and the occasional set of conditions where the water and acetonitrile components underwent phase separation.

Results

Chemical Reduction and Protonation. The singly ($\mathbf{P}^-$) and doubly ($\mathbf{P}^{2-}$) reduced forms of **P** were generated in situ via stoichiometric reductions with cobaltocene in acetonitrile, and their absorption spectra are shown in Figure 2a. Cobaltocene is a strong one-electron reducing agent (−1.0 V vs Ag/AgCl in acetonitrile)[18] and thermodynamically capable of generating both $\mathbf{P}^-$ and $\mathbf{P}^{2-}$ ($E_{1/2}$ of −0.22 and −0.71 V vs Ag/AgCl, respectively) but not $\mathbf{P}^{4-}$ ($E_{1/2} = -1.28$ V (vide infra)). The cobaltocenium ion produced is light yellow in color and adds no appreciable absorption[19] to the visible and near-IR portion (350−1100 nm) of the absorption spectra. Both $\mathbf{P}^-$ and $\mathbf{P}^{2-}$ show new, strong ligand-centered (LC) bands in the visible and near-IR portion of the spectrum. Formation of $\mathbf{P}^-$ yields two new absorptions in the near-IR at 860 nm (weak) and 970 nm (strong) which appear to be vibronic bands of the central reduced aromatic unit (tatpp radical anion) plus a partial bleaching of the absorption at 325 nm. We also observe that the maximum of the 445 nm peak in **P** is blue shifted to 415 nm; however, a strong shoulder remains at 445 nm which is attributed to the Ru-phen type MLCT. Addition of a second equivalent of cobaltocene generates $\mathbf{P}^{2-}$ and results in a blue shift of the near-IR peaks to give a strong band at 685 nm with a shoulder at 635 nm (see Figure 2a). This second reduction also results in the complete bleaching of the tatpp LC bands at 325 and 445 nm.

The absorption spectra for protonated complexes $\mathbf{HP}^-$ and $\mathbf{H_2P}$, formed by addition of 1 or 2 equiv of TFA to $\mathbf{P}^{2-}$, respectively, are shown in Figure 2b. The most noticeable change upon formation of $\mathbf{HP}^-$ is the appearance of a third band at 725 nm and a slight blue shift of the nearby bands to 655 and 608 nm (sh). Addition of the second proton gives $\mathbf{H_2P}$ which has a broad, strong absorption centered at 580 nm. We note that the process is reversible and that stepwise deprotonations of $\mathbf{H_2P}$ with NaOMe yielded the spectra for $\mathbf{HP}^-$ and $\mathbf{P}^{2-}$, respectively. $\mathbf{H_2P}$ can also prepared by reduction with excess $NaBH_4$ in acetonitrile and 5% acetic acid, and spectroscopic monitoring of this process shows no sign of any singly reduced intermediates. The UV−visible spectroscopic data for the complexes are gathered in Table 1.

Protonation of $\mathbf{P}^-$ with TFA presumably would yield **HP**; however, the resulting absorption spectrum, shown in Figure 2c, suggests that **HP** may disproportionate as indicated in reaction 1. We observe two features in the spectrum of **HP**

$$2\mathbf{P}^- + 2H^+ \rightarrow 2\text{“}\mathbf{HP}\text{”} \rightarrow \mathbf{P} + \mathbf{H_2P} \qquad (1)$$

supporting this hypothesis: a strong, broad absorption characteristic of $\mathbf{H_2P}$ at 580 nm, and the reappearance of some intensity to the bands at 445 and 325 nm characteristic of **P**. For comparison, the spectra of **P** and $\mathbf{H_2P}$ at the same molar concentration are overlaid with that of "**HP**" in Figure 2c. The fact that the peak at 580 nm for "**HP**" is one-half as intense as the same peak observed in a pure sample of $\mathbf{H_2P}$ is particularly revealing. Also, a 1:1 mixture of **P** and $\mathbf{H_2P}$ gives the same spectrum as **HP**. So either these two do react to give **HP**, which coincidentally has a spectrum much like the sum of its components, or the two do not comproportionate and the resulting spectrum is simply that of the 1:1 mixture. The latter explanation seems far more reasonable, especially when one considers that a 400 nm blue shift of the peaks in the near-IR

(17) Jang, G.-W.; Tsai, E. W.; Rajeshwar, K. *J. Electrochem. Soc.* **1987**, *134*, 2377−2380.

(18) Gubin, S. P.; Smirnova, S. A.; Denisovich, L. I. *J. Organomet. Chem.* **1971**, *30*, 257−265.

(19) Koelle, U.; Infelta, P. P.; Gratzel, M. *Inorg. Chem.* **1988**, *27*, 879−883.

Table 1. Spectroscopic Data of the Dimeric Complexes in Deaerated Acetonitrile

compound	absorption at 298 K, λ_{max}, nm (ϵ, M^{-1} cm^{-1})
$[(phen)_2Ru(tatpp)Ru(phen)_2]^{4+}$ (**P**)	325 (72 900), 425 sh (42 600), 445 (54 300)
$[(phen)_2Ru(tatpp^{-})Ru(phen)_2]^{3+}$ (**P**$^{-}$)	325 sh (37 600), 415 (54 800), 445 sh (46 100), 860 (14 100), 970 (35 600)
$[(phen)_2Ru(tatpp^{2-})Ru(phen)_2]^{2+}$ (**P**$^{2-}$)	430 sh (40 000), 445 (41 900), 635 (25 900), 685 (55 400)
$[(phen)_2Ru(Htatpp^{-})Ru(phen)_2]^{4+}$ (**HP**$^{-}$)	418 (43 600), 444 sh (38 000), 608 (27 600), 655 (38 000), 725 (43 600)
$[(phen)_2Ru(H_2tatpp)Ru(phen)_2]^{4+}$ (**H_2P**)	580 (37 400), 445 (34
$[(phen)_2Ru(tatpp^{4-})Ru(phen)_2]$ (**P**$^{4-}$)	448 (23 400)

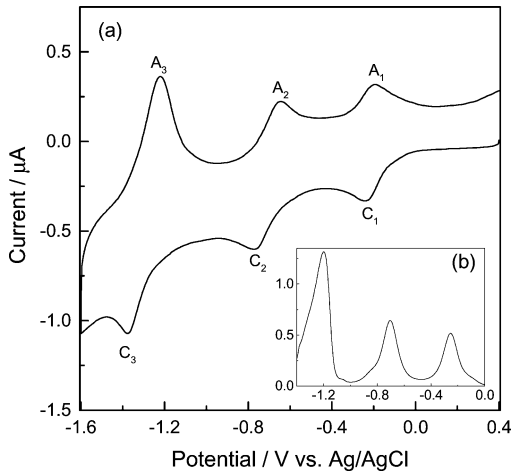

Figure 3. Cyclic (a) and differential pulse (b) voltammograms of 0.03 mM **P** in acetonitrile containing 0.1 M $NBu_4^nPF_6$. (a) Potential scan rate = 50 mV/s. (b) Pulse amplitude = 0.05 V, step size = 0.004 V, pulse duration = 0.05 s, and pulse period = 0.2 s. The working electrode for both measurements was a glassy carbon disk (1.5 mm diameter).

to give a new maximum at 580 nm upon a single protonation step is unlikely.[20,21]

Cyclic Voltammetry and Spectroelectrochemistry of P in Acetonitrile. The cyclic voltammogram for 0.03 mM **P** in 0.1 M $NBu_4^nPF_6$−acetonitrile solution in the potential region from 0.4 to −1.6 V is shown in Figure 3. The voltammetric scan was started at 0.4 V and scanned in the negative direction down to −1.6 V. Three quasi-reversible tatpp-centered reductions are observed and are indicated as A_1/C_1, A_2/C_2, and A_3/C_3 in the voltammogram. These voltammetric peaks reflect two mono- and one bi-electronic processes with $E_{1/2}$ potentials of −0.22, −0.71, and −1.28 V vs Ag/AgCl, respectively. Previously, we reported that the third (bi-electronic) process was not reversible and half-wave potentials were −0.18 and −0.56 V for the $A_1/C_1$and A_2/C_2 processes, respectively.[13] The discrepancy appears to be a concentration/aggregation effect which is not uncommon for this class of compounds. Our earlier reported data were based on measurements made with 0.5 mM **P** solutions and are reproducible under these conditions. Only upon dilution of the solution (0.03 mM **P** in this work) do we observe the voltammogram presented in Figure 3. DPV data (see Figure 3, inset) corroborate the information provided by CV and show the A_3/C_3 process to involve twice as many electrons as the other two. Not shown are an additional reduction process at ca. −1.92 V, which is likely related to the reduction of the terminal phenanthroline ligands, and a bielectronic oxidative process at +1.36 V corresponding to two weakly coupled $Ru^{2+/3+}$ centers.

Figure 4 shows how the absorption spectra of **P** evolve during a CV performed at 5 mV/s in 0.1 M $NBu_4^nPF_6$−acetonitrile solution and scanning in the potential window shown in Figure 3 starting at +0.4 V. The top three frames (Figure 4a−c) correspond to the negative-going scan, and the three frames at the bottom (Figure 4d−f) were obtained during the subsequent positive-going scan. The arrows in each frame indicate the evolution of the corresponding spectral peaks, and it is clearly seen that for those frames aligned vertically, virtually identical processes occur, only in opposite directions.

Describing each frame in detail, we can see that, in Figure 4a, the first spectrum corresponds to **P** (bearing a dark yellow color) as the starting material with a sharp band at 445 nm and a small shoulder at 425 nm. During the first electroreduction process (voltammetric peak C1), the sharp band at 445 nm (which we now recognize as a signature peak for **P**) decreases at the expense of the development of three spectral peaks: a rather broad signature at 415 nm and a pair of sharper bands at 860 and 970 nm. This spectrum is virtually identical with that obtained by cobaltocene reduction of **P** to **P**$^{-}$ (see Figure 2a) and corroborates that the two processes yield the same product. Despite the large spectral changes (mostly in the near-IR), we note that the solution does not undergo a visible color change during this process and maintains a yellow hue throughout this first process.

Figure 4b shows the spectral evolution encompassing voltammetric peak C_2, with a visible yellow-to-green transformation. Spectrally, we observe that the band pair at 860 and 970 nm is converted into another pair at 635 and 685 nm, respectively. Again, the agreement of the cobaltocene reduction data is clear, indicating that these latter peaks are associated with formation of **P**$^{2-}$.

In the third potential region (Figure 4c) and encompassing the voltammetric peak C_3, all the spectral features from Figure 4b are seen to decrease significantly in intensity, bringing about a bleaching of the green solution color to a pale yellow hue. There is an almost complete disappearance of the band pair at 635 and 685 nm, leaving only a broad band at 445 nm of low intensity. The bands at 635 and 685 nm are likely to be associated with LC transitions of the doubly reduced $tatpp^{2-}$ ligand (in **P**$^{2-}$). The fact that these two peaks are bleached upon an additional two-electron reduction (see Figure 4c) suggests that the $tatpp^{2-}$ bridging ligand is reduced to $tatpp^{4-}$. Such extensive reduction of the tetraazapentacene framework would disrupt any extended conjugation across the tatpp ligand and could easily be expected to bleach any low-energy LC transitions. This last redox process, reduction of **P**$^{2-}$ to **P**$^{4-}$, has never been observed in the photochemical process. As shown in frames d, e, and f of Figure 4, the three reductive processes are completely reversible, and all of the redox intermediates are seen to reappear and disappear in order until **P** is completely regenerated.

The potentials at which the various species appear and disappear in the spectroelectrochemical experiment can be

(20) Long, C.; Vos, J. G. *Inorg. Chim. Acta* **1984**, *89*, 125−131.
(21) Haga, M.-A. *Inorg. Chim. Acta* **1983**, *75*, 29−35.

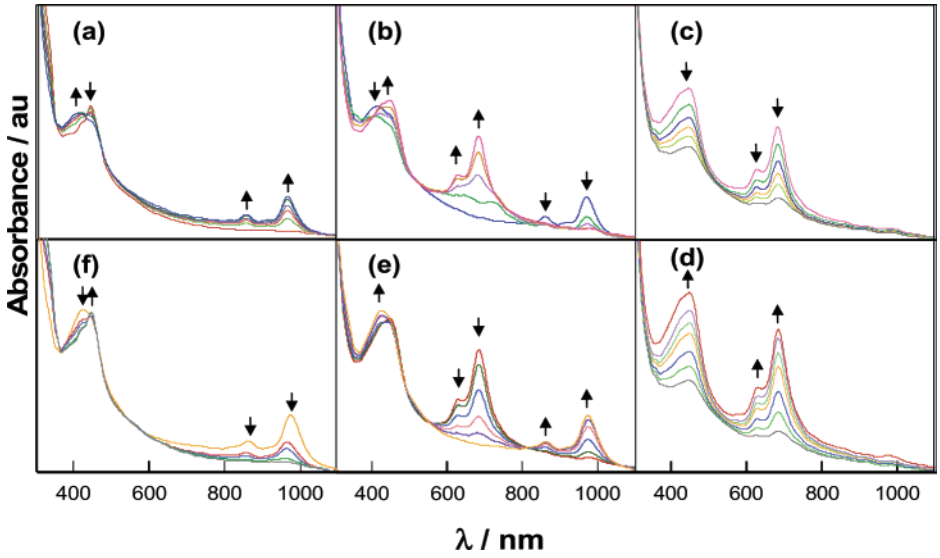

Figure 4. Spectroelectrochemistry of 0.02 mM **P** in acetonitrile containing 0.1 M $NBu_4^nPF_6$ using a capillary slit cell. Spectra were collected during a cyclic potential scan at 5 mV/s in the 0.4 to −1.6 V potential range. For the sake of clarity, only a selected subset of spectra is shown during a negative- (a−c) and positive-going (d−f) potential scan direction.

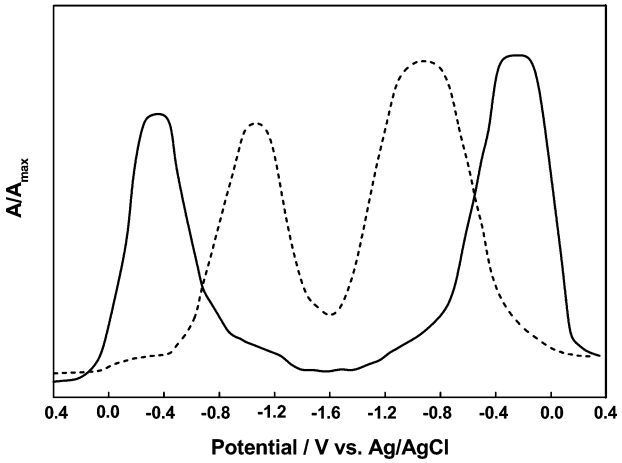

Figure 5. Evolution as a function of potential of bands peaking at 970 nm ($\mathbf{P}^-$; solid line) and at 685 nm ($\mathbf{P}^{2-}$; dashed line). The *y*-axis is presented as normalized absorbance, A/A_{max}, for each band. Data were obtained from the spectra depicted in Figure 4.

correlated with the CV data by plotting the normalized intensity for the peak at 970 nm ($\mathbf{P}^-$) and at 685 nm ($\mathbf{P}^{2-}$) as a function of the electrode potential, as shown in Figure 5. We observe that the peak associated with $\mathbf{P}^-$ reaches a maximum at ca. −0.3 V (vs $E_{1/2}(\mathbf{P}^{0/-}) = -0.22$ V in the CV data). The slightly more negative potential for the spectroelectrochemical data is not unreasonable since not all the complex **P** is reduced at the $E_{1/2}$. As the potential increases more negatively, we observe the appearance of a peak at 685 nm ($\mathbf{P}^{2-}$) at the expense of the 970 nm peak, reaching a maximum at −1.0 V (vs −0.71 V for the $E_{1/2}$ for $\mathbf{P}^{-/2-}$). Finally, at potentials more negative than −1.0 V, the 685 nm peak begins to bleach, indicating formation of $\mathbf{P}^{4-}$ ($E_{1/2}(\mathbf{P}^{2-/4-}) = -1.28$ V). At −1.6 V, the scan is reversed and $\mathbf{P}^{2-}$ and then $\mathbf{P}^-$ are seen to reappear and disappear in order until **P** is regenerated at +0.4 V. The intensities of the 685 and 970 nm peaks are rather higher on the return (positive-going) scan, which indicates that the electroreduction processes continued forming $\mathbf{P}^{4-}$ even during the switch of the potential scan at −1.6 V, thus providing a higher yield of $\mathbf{P}^{2-}$ and then $\mathbf{P}^-$ during the positive-going scan.

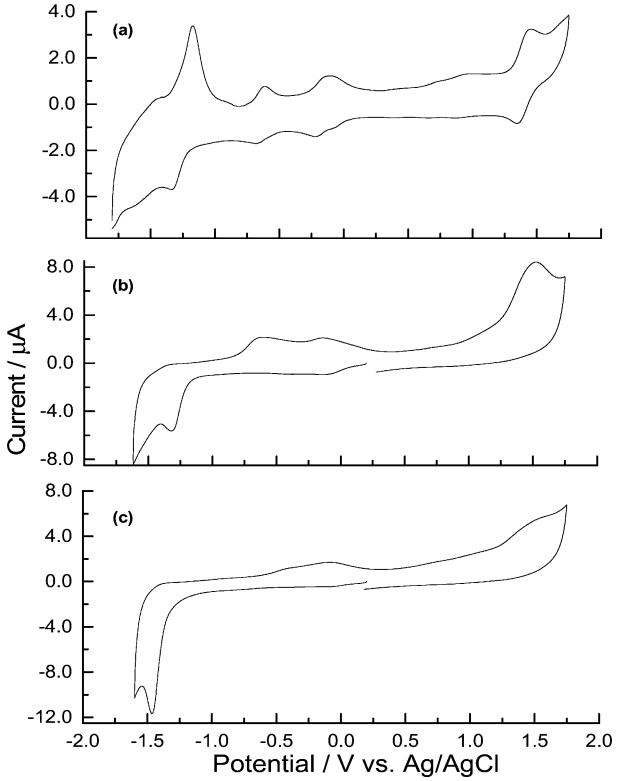

Figure 6. Effect of water on the cyclic voltammograms of **P**: (a) 0.5% water, (b) 10% water, and (c) 20% water. These voltammograms were obtained at 50 mV/s with a glassy carbon disk (diameter = 1.5 mm) in 0.2 mM **P** in acetonitrile containing 0.1 M $NBu_4^nPF_6$. The solutions were purged with argon for 30 min before recording the voltammograms.

Aqueous Electrochemistry and Spectroelectrochemistry. The reversibility of the electrochemical processes is strongly affected by added water, as shown in Figure 6. All four redox processes (left to right: $\mathbf{P}^{4-/2-}$, $\mathbf{P}^{2-/-}$, $\mathbf{P}^{-/0}$, $Ru^{2+/3+}$) are still clearly observed upon addition of 0.5% water (Figure 6a); however, the processes are noticeably less reversible (ΔE_{p-p} of 99.8, 80.1, and 175 mV for processes C_1/A_1, C_2/A_2, and C_3/A_3, respectively), and the C_1 peak begins to split. In a 10% water−acetonitrile solution (Figure 6b), all of the redox

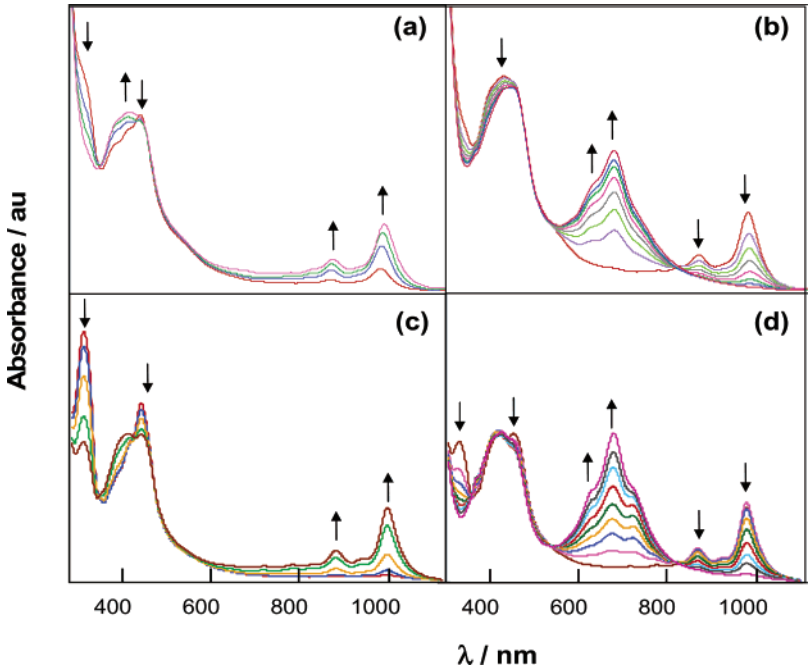

Figure 7. Spectroelectrochemistry of **P** in 20% water−acetonitrile at pH 12 (a,b) and 9.5 (c,d). Frames a and c correspond to the first electroreduction process, and frames b and d to the second electroreduction process at the corresponding pH's. Spectra were collected during a cyclic potential scan at 5 mV/s, but only those obtained during the negative-going potential scan are shown in this figure for the sake of clarity.

processes are still discernible, but none are reversible, and at 20% water in acetonitrile (Figure 6c), the two peaks associated with $\mathbf{P}^{2-/-}$ and $\mathbf{P}^{-/0}$ couples are barely observed and have shifted to slightly more positive potentials. As the photochemical activity is still observed in 20% water−acetonitrile (vide infra) and the individual redox processes are still discernible in the CV, we chose to examine the spectroelectrochemistry of **P** in this mixture. The solution pH, as recorded by a standard glass electrode, was varied in order to examine the range of species that could be formed in the presence of water.

Figure 7 compares spectroelectrochemical data at pH 12 and 9.5 as obtained during a potential scan from 0.4 to −1.6 V. The columns of the left (Figure 7a,c) show the initial one-electron reduction product, and the columns on the right (Figure 7b,d) show the disappearance of the one-electron product and appearance of the doubly reduced product. At pH 12 (Figure 7a,b), we can assign the one-electron reduction product as $\mathbf{P}^{-}$ and the two-electron product as a mixture of mainly $\mathbf{P}^{2-}$ and some $\mathbf{HP}^{-}$. At pH 9.5 (Figure 7c,d), unprotonated $\mathbf{P}^{-}$ is still the favored one-electron product, whereas $\mathbf{HP}^{-}$ is the dominant form of the doubly reduced product (as judged by the appearance of the 725 nm peak, see Figure 7d), with some $\mathbf{P}^{2-}$ still apparent as the 725 nm feature is not fully developed (see Figure 2b).

Contrasting with the previous spectroelectrochemical profiles, an interesting change in the absorption spectra of the singly reduced product was observed at pH 7 (Figure 8a). Some $\mathbf{P}^{-}$ is initially formed, as indicated by the appearance of the 970 nm band, but this peak quickly reaches a maximum at a value much less than that observed at higher pH (see Figure 7a,c). As the band at 970 nm approaches its maximum value, a new broad peak at 580 nm begins to appear which is consistent with the appearance of $\mathbf{H_2P}$ (also Figure 8a). The relatively rapid appearance of this peak under potentials where only the singly reduced product is formed at higher pH (see Figure 7a,c) could be explained by protonation of $\mathbf{P}^{-}$ to **HP** and, once an

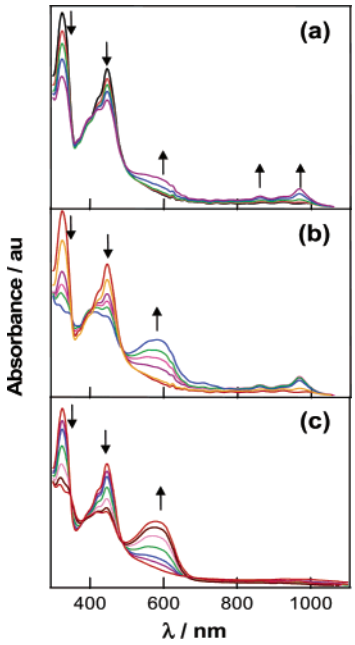

Figure 8. Spectroelectrochemistry of **P** in 20% water−acetonitrile at pH 7 (a,b) and pH 4 (c). The potential window was 0.4 to −1.6 V for pH 7 and 0.4 to −1.4 V for pH 4. Others details as in Figure 7.

appreciable concentration of HP is generated, a disproportionation to $\mathbf{H_2P}$ and **P** (reaction 1). Any **P** formed in the disproportionation reaction would be immediately re-reduced by the electrode, and thus the $\mathbf{H_2P}$ is the only stable product obtainable under these conditions. As the electrode is biased more negatively, we eventually see the rapid appearance of the 580 nm peak associated with $\mathbf{H_2P}$ and the complete bleaching of the 325 nm peak associated with **P** (Figure 8b).

As shown in Figure 8c, the spectroelectrochemistry of **P** at pH 4 shows only the appearance of the doubly reduced product $\mathbf{H_2P}$ and no trace of the one-electron products $\mathbf{P}^{-}$ or **HP**. The

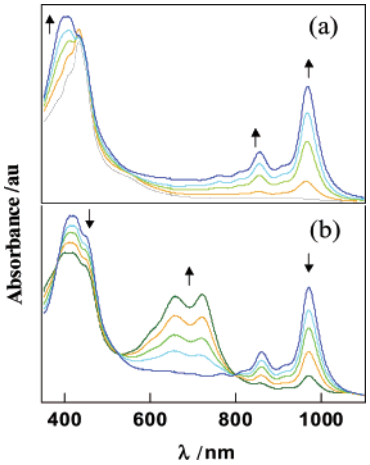

Figure 9. Evolution of the visible spectrum of 16 μM **P** in deaerated acetonitrile containing 0.25 M TEA during photoirradiation: (a) 0−2 min and (b) 2−12 min.

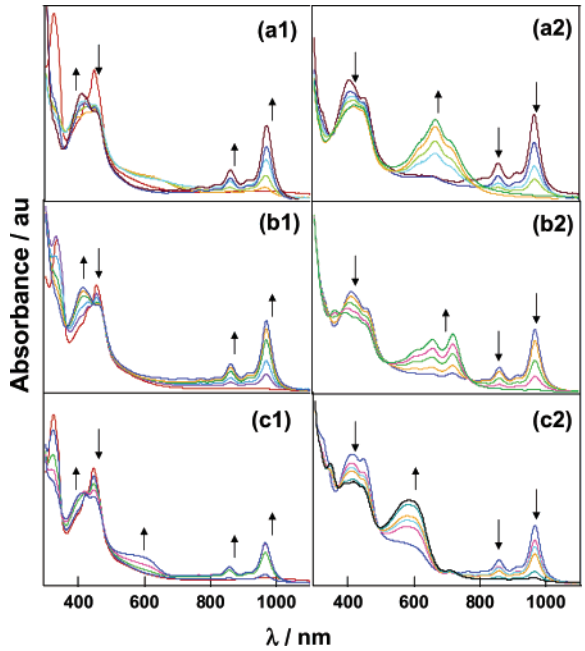

Figure 10. Evolution of the visible spectrum of 16 μM **P** in deaerated 20% water−acetonitrile: pH 12 (a), pH 10 (b), and pH 8 (c). Frames numbered with a 1 correspond to the initial irradiation period (approximately 3−6 min long) and frames with a 2 correspond to the appearance of a distinct second photoproduct over the time period ranging from 3 to 15 min.

clean isosbestic points at 345, 380, and 490 nm show that **P** undergoes a concerted two-proton, two-electron reduction at this pH. Identical behavior is observed for the chemical reduction of **P** to $\mathbf{H_2P}$ with excess $NaBH_4$ in 20% water−acetonitrile at pH 4.

Photochemistry in Acetonitrile. Visible irradiation of **P** results in the appearance of two photoproducts, as shown in Figure 9a,b. Under these conditions, it is known that protons are generated in solution via the thermal decomposition of the coproduct, the TEA radical cation,[22] leading to uncertainty in the protonation state of the two products. We note that the first trace is for the spectrum of **P** without added TEA and the second trace with the added TEA already shows the formation of a small amount of $\mathbf{P}^-$ even prior to irradiation. This represents either a small but reversible thermal reaction or a charge-transfer complex between the TEA and **P**. Higher concentrations of TEA can lead to a complete thermal reduction of **P** to $\mathbf{P}^-$ but no further. We chose a concentration of 0.25 M TEA because here only a small amount of thermal reactivity is observed and the photochemical reaction still proceeds rapidly. Once $\mathbf{P}^-$ is fully formed, continued irradiation leads to the gradual disappearance of the $\mathbf{P}^-$ peaks and the appearance of three new bands at 725, 655, and 608 nm (Figure 10b), which are characteristic of the singly protonated, doubly reduced $\mathbf{HP}^-$. A comparison of the absorption data with those obtained by stoichiometric chemical reduction and protonation corroborates these assignments.

Photochemistry in Mixed Water−Acetonitrile. The photochemical activity of **P** is maintained when water is added to the system. Specifically, we examined the photochemistry of **P** in thoroughly degassed solutions of 20% water−acetonitrile at different pH values to mimic the spectroelectrochemical conditions. In general, the spectra obtained photochemically, shown in Figure 10, closely match those obtained by electroreduction at similar pH; however, no photochemical activity was observed at pH 7 or below. At each of the three pH's examined, two distinct photoproducts are observed sequentially and are clearly assignable to one- and two-electron reduced products. At pH 12 and 10 (Figure 10a1,a2,b1,b2), the first photoproduct is $\mathbf{P}^-$. At pH 8, we observe an additional band at 580 nm during the first reduction which we attribute to formation of $\mathbf{H_2P}$, presumably via the disproportionation of a small amount of **HP** generated from protonation of $\mathbf{P}^-$ at this pH. However, once all the **P** is consumed, we observe complete conversion of the remaining $\mathbf{P}^-$ to $\mathbf{H_2P}$ (Figure 10c2). The photochemical activity is not always as well behaved as the spectroelectrochemical data, as typified by the lack of clear isosbestic points in the data collected at pH 12.

Discussion

We have identified seven distinct species of **P**, depicted in Figure 1, that are interlinked by electron transfer and/or protonation/deprotonation processes. Of these, only $\mathbf{P}^{4-}$ does not play a role in the photochemistry of **P**, and only **HP** appears to be unstable with respect to disproportionation. Fortunately, all of these species show unique absorption spectra, which provide a quick and reliable way to determine both the oxidation and protonation states of **P** in solution. It is also the absorption data, summarized in Table 1, which provide the common link between the titration, spectroelectrochemical, and the photochemical data.

In an attempt to understand the underlying electronic reasons for the observed spectral changes, we examined the absorption spectra in detail. As is common to these types of complexes, the absorption spectra of the species in Figure 1 in acetonitrile are dominated by very intense spin-allowed ligand-centered (LC) transitions in the UV and visible region and by intense spin-allowed metal-to-ligand charge-transfer (MLCT) transitions in the visible. In particular, all the species show broad bands around 445 nm which are similar in energy and shape to the lowest-energy absorption band of $[Ru(phen)_3]^{2+}$ and can be assigned, in part, to the spin-allowed $Ru(d\pi) \rightarrow phen(\pi^*)$ MLCT transition, which is responsible for the luminescent behavior of

(22) DeLaive, P. J.; Foreman, T. K.; Giannotti, C.; Whitten, D. G. *J. Am. Chem. Soc.* **1980**, *102*, 5627−5631.

$[Ru(phen)_3]^{2+}$.[23−25] These MLCT bands are constant throughout all the spectra and are not bleached upon reduction. From its structured shape and high molar extinction coefficient, it is clear that the band at 445 nm for **P** also receives contributions from a LC ($\pi \rightarrow \pi^*$) transition involving the tatpp bridging ligand. The 445 nm band in **P** has a molar absorptivity of 54 250 cm^{-1} M^{-1} compared to the anticipated molar absorptivity at 450 nm for two $[Ru(phen)_3]^{2+}$ MLCTs of 36 000 cm^{-1} M^{-1}. As the extinction coefficients for weakly coupled MLCTs are generally additive,[26] we can assign the "extra" molar absorptivity of ca. 18 250 cm^{-1} M^{-1} to a tatpp LC transition. A second LC band is observed at 325 nm and is assigned to a tatpp $\pi-\pi^*$ transition, as this peak is absent in $[Ru(phen)_3]^{2+}$. Chiorboli, Gourdon, and co-workers have observed a similar overlap of low-energy LC bands (n$-\pi^*$, $\pi-\pi^*$) with the Ru-phen MLCT in related TPPHZ and bpy-pyrene-bpy bridged dimers.[27−30] Upon reduction, we observe the bleaching or movement of these LC transitions and see new LC bands that are characteristic of the reduced forms of the parent hydrocarbon, tetraazapentacene.[15] We note that vibrational fine structure is seen as associated peaks or shoulders for the LC transitions in most of the complexes and that the energy difference between the first and second vibronic states is approximately constant at 1330 cm^{-1} for **P** (445 and 425 nm), 1320 cm^{-1} for $\mathbf{P}^-$ (860 and 970 nm), and 1242 cm^{-1} for $\mathbf{P}^{2-}$ (635 and 685 nm), as would be expected for aromatic ring breathing modes.[31−35] The slight decrease in vibrational energy upon going from **P** to $\mathbf{P}^-$ to $\mathbf{P}^{2-}$ is consistent with reduction of the tetraazapentacene unit.

A qualitative but fully self-consistent interpretation of these data is obtained by expanding on the MO picture developed previously for **P**.[16] Figure 11 shows a MO energy level diagram in which we adopt a localized view of the electron distribution in which three tatpp-based orbitals, the HOMO−1 (π), LUMO (π_0^*), and LUMO+1 (π_1^*), and one metal-based orbital, the HOMO (dπ), play significant roles in the visible absorption spectra. As with related DPPZ[36,37] and TPPHZ[36,38] type complexes, we can attribute the various MOs as being largely localized on specific portions of the tatpp ligand and being "bipyridine-like" (π_1^*) or "tetraazapentacene-like" (π and π_0^*).

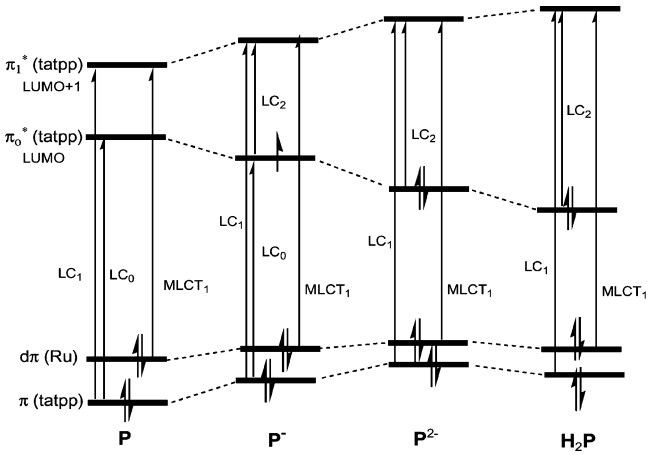

Figure 11. Qualitative molecular orbital energy diagram showing the important optical transitions and orbitals involved for related redox and protonation isomers of **P**.

For **P** (Figure 11, far left), three of four possible transitions, labeled LC_1, LC_0, and $MLCT_1$, would correspond to the peaks at 325 nm and two overlapping sharp and broad transitions at 445 nm, respectively. The overlap of the LC_0 and $MLCT_1$ transitions is apparent by the structured narrow peak (LC_0) and the latter being the usual broad transition between 440 and 480 nm typically observed for Ru(dπ) $\rightarrow$ bipyridine(π_1^*) type transitions ($MLCT_1$). In this case, the π_1^* "bipyridine-like" acceptor orbital on tatpp is strongly coupled to the Ru(dπ) orbitals and is the site initially populated upon MLCT. Importantly, the possible $MLCT_0$ transition, Ru(dπ) $\rightarrow$ tatpp(π_0^*), is not observed, which is typical for this and related DPPZ and TPPHZ complexes and is related to the poor electronic coupling of the dπ and π_0^* orbitals.[29,30,36−39]

Upon reduction to $\mathbf{P}^-$, the π_0^* orbital is singly populated and a new transition, LC_2, becomes possible which we assign to a pair of vibronic peaks at 860 and 970 nm. The energy of the ν_{0-0} band ($\sim$10 300 cm^{-1}) in $\mathbf{P}^-$ is reasonably close to the estimated energy difference between these two levels in **P** ($LC_1-LC_0 \approx 8300$ cm^{-1}), considering the expected increase in ΔE between π_1^* and π_0^* upon reduction. Addition of a second electron to form $\mathbf{P}^{2-}$ would fill the π_0^* orbital and lead to additional nuclear rearrangement to stabilize the π_0^* at the expense of the π_1^* orbital. This would result in a further blue shift of the LC_2 transition. There is a clear shift of the vibronic pair associated with LC_2 from 860, 970 nm in $\mathbf{P}^-$ to 635, 685 nm in $\mathbf{P}^{2-}$, consistent with this interpretation. The fact that the first reduction leads to an apparent red shift of the 445 nm peak to 970 nm and the second reduction results in a blue shift to 685 nm suggests they are not the same type of transition, as is suggested in our model with LC_0 assigned to the 445 nm in **P** and LC_2 assigned to the transitions at 970 and 685 nm in $\mathbf{P}^-$ and $\mathbf{P}^{2-}$, respectively. The bleaching of the 325 nm peak (LC_1) in $\mathbf{P}^-$ and $\mathbf{P}^{2-}$ is likely due to a blue shift outside our spectral window (<300 nm) and would be expected from the model in Figure 11.

Assuming protonation further stabilizes the now full π_0^* orbital in $\mathbf{P}^{2-}$, we could expect that $\mathbf{HP}^-$ and $\mathbf{H_2P}$ should show a continued blue shift in the LC_2 transitions. For $\mathbf{H_2P}$, this is clearly seen by the appearance of the broad band at 580 nm at

(23) Crosby, G. A.; Perkins, W. G.; Klassen, D. M. *J. Chem. Phys.* **1965**, *43*, 1498−1503.
(24) Lytle, F. E.; Hercules, D. M. *J. Am. Chem. Soc.* **1969**, *91*, 253−257.
(25) Demas, J. N.; Crosby, G. A. *J. Mol. Spectrosc.* **1968**, *26*, 72−77.
(26) MacDonnell, F. M.; Ali, M. M.; Kim, M.-J. *Comments Inorg. Chem.* **2000**, *22*, 203−225.
(27) Ishow, E.; Gourdon, A.; Launay, J.-P.; Lecante, P.; Verelst, M.; Chiorboli, C.; Scandola, F.; Bignozzi, C.-A. *Inorg. Chem.* **1998**, *37*, 3603−3609.
(28) Ishow, E.; Gourdon, A.; Launay, J.-P.; Chiorboli, C.; Scandola, F. *Inorg. Chem.* **1999**, *38*, 1504−1510.
(29) Chiorboli, C.; Bignozzi, C.-A.; Scandola, F.; Ishow, E.; Gourdon, A.; Launay, J.-P. *Inorg. Chem.* **1999**, *38*, 2402−2410.
(30) Bolger, J.; Gourdon, A.; Ishow, E.; Launay, J.-P. *Inorg. Chem.* **1996**, *35*, 2937−2944.
(31) Caspar, J. V.; Westmoreland, T. D.; Allen, G. H.; Bradley, P. G.; Meyer, T. J.; Woodruff, W. H. *J. Am. Chem. Soc.* **1984**, *106*, 3492−3500.
(32) Chang, Y. J.; Xu, X.; Yabe, T.; Yu, S. C.; Anderson, D. R.; Orman, L. K.; Hopkins, J. B. *J. Phys. Chem.* **1990**, *94*, 729−736.
(33) Bradley, P. G.; Kress, N.; Hornberger, B. A.; Dallinger, R. F.; Woodruff, W. H. *J. Am. Chem. Soc.* **1981**, *103*, 7441−7446.
(34) Mabrouk, P. A.; Wrighton, M. S. *Inorg. Chem.* **1986**, *25*, 526−531.
(35) Jaffe, H. H.; Orchin, M. *Theory and Application of Ultraviolet Spectroscopy*; Wiley: New York, 1964.
(36) Pourtois, G.; Beljonne, D.; Moucheron, C.; Schumm, S.; Kirsch-De Mesmaeker, A.; Lazzaroni, R.; Bredas, J.-L. *J. Am. Chem. Soc.* **2004**, *126*, 683−692.
(37) Brennaman, M. K.; Alstrum-Acevedo, J. H.; Fleming, C. N.; Jang, P.; Meyer, T. J.; Papanikolas, J. M. *J. Am. Chem. Soc.* **2002**, *124*, 15094−15098.
(38) Chiorboli, C.; Rodgers, M. A. J.; Scandola, F. *J. Am. Chem. Soc.* **2003**, *125*, 483−491.
(39) Campagna, S.; Serroni, S.; Bodige, S.; MacDonnell, F. M. *Inorg. Chem.* **1999**, *38*, 692−701.

the expense of the peaks at 635 and 685 nm. Upon protonation of $\mathbf{P}^{2-}$ to $\mathbf{HP}^{-}$, the vibronic pair at 630, 685 nm blue shifts to 608, 655 nm, which is smaller than that observed with $\mathbf{H_2P}$, as expected, and a new low-energy transition at 725 nm is observed. The origin of this last transition is less clear, but it is clearly diagnostic of monoprotonation of $\mathbf{P}^{2-}$. While this model does not explain all the observed spectral changes, the gross changes in the LC transitions seem adequately represented in this picture.

Spectroelectrochemistry and Photochemistry. Complex **P** is photochemically active but it is not luminescent.[16] This result has been interpreted as efficient quenching of the (inherently emissive) $^3MLCT_1$ excited state by triplet−triplet energy transfer to a $^3MLCT_0$ state involving population of the LUMO (π_0*).[16] Another way to view this process is as an intramolecular electron transfer between a weakly coupled "bipyridine-like" unit and a central "tetraazapentacene-like" unit. This latter view emphasizes the spatial separation of the electron−hole pair. As mentioned previously, the $^3MLCT_0$ state is poorly coupled with the Ru dπ orbital, which apparently leads to long-lived excited states and ultimately to facile reduction of the transient Ru^{3+} center by the sacrificial reductant. While reductive quenching of a photoexcited Ru-bpy type chromophore is not unusual for a single reduction, the ability to repeat this process and doubly reduce the acceptor orbital is unprecedented. A similar situation with a different outcome is seen in the related dimer, $[(bpy)_2Ru(bddpz)Ru(bpy)_2]^{4+}$ (where bdppz is the bridging bis-DPPZ ligand, 1,1′-dipyrido[3,2-*a*:2′,3′-*c*]phenazine), in which all luminescent activity (as opposed to photochemical activity) is lost upon reduction to $[(bpy)_2Ru(bddpz^{\bullet-})Ru(bpy)_2]^{3+}$.[40] In this case, the presumed mechanism of quenching is rapid intramolecular reduction of the excited [Ru(III)($bpy^{\bullet-}$)] fragment by the bridging $bddpz^{\bullet-}$ radical anion. The observed reduction potential for the $\mathbf{P}^{-/2-}$ couple at −0.71 V suggests that the $tatpp^{\bullet-}$ ligand will still be the preferred site of charge injection, considering that reduction of the terminal phen ligands comes at far more negative potentials (ca. −1.9 V). Protonation of the central tetraazapentacene nitrogens (formation of **HP**) would relieve some of the Coulombic repulsion during the second charge injection, but it does not appear to be an absolute necessity, as the second photochemical reduction occurs readily in 20% water−acetonitrile at pH 12 and yields mainly $\mathbf{P}^{2-}$. Clearly, the unusual electronic structure tatpp ligand in which the MLCT acceptor orbital (π_1*) is not the ultimate site of electron storage is key to this behavior. Currently, we are unsure if the loss of photochemical activity at pH 7.5 or below is due to deactivation of **P** or loss of free TEA through formation of triethylammonium ion. The observation of clean two-electron, two-proton reductions at lower pH's (by both chemical and electrochemical means) may signal a change in the reduction/protonation mechanisms involved and also highlights the ability of **P** to participate in concerted two-electron processes.

While the multielectron photoreduction of **P** in acetonitrile is intriguing and important, it is the retention of this multielectron photochemical activity in the presence of water that really shows promise from a practical standpoint. We observe two distinct photoproducts in water−acetonitrile (1:4, pH > 7.5) solution whose absorption spectra are virtually identical to those generated by sequential electroreduction under similar solvent conditions. Furthermore, a comparison of the absorption spectra with those obtained in acetonitrile clearly indentify the photoproducts as one- and two-electron-reduced species. The photochemical activity in the presence of water is surprising because protic solvents efficiently quench the luminescent activity of the closely related DPPZ and TPPHZ[28−30,38,39,41] complexes of Ru(II). We are currently using time-resolved absorption spectroscopy to elucidate these unusual photophysical properties and will communicate these results separately.

Regardless of the detailed photophysics of **P**, we observe that it is possible to couple protonation with photoreduction, a feature that has been proposed as essential in most natural light-activated energy-storing processes.[42,43] Most importantly, we can photochemically generate $\mathbf{H_2P}$ at pH 8, which carries two protons and two electrons, or effectively one H_2 molecule, within its structure. We are currently exploring methods of dehydrogenating this complex in order to establish a catalytic cycle in which hydrogen is produced.

Acknowledgment. This work was supported by the NSF CHE-0101399 (F.M.M.), ACS-PRF, Type AC (F.M.M., K.R.), Robert A. Welch Foundation (F.M.M.), and Sigma Xi-GIAR fellowship (R.K.). We thank Professors Sebastiano Campagna and Franco Scandola for useful comments and discussions.

JA047931L

(40) Staffilani, M.; Belser, P.; De Cola, L.; Hartl, F. *Eur. J. Inorg. Chem.* **2002**, *2*, 335−339.
(41) Bolger, J.; Gourdon, A.; Ishow, E.; Launay, J.-P. *J. Chem. Soc., Chem. Commun.* **1995**, 1799−1800.
(42) Tommos, C.; Babcock, G. T. *Acc. Chem. Res.* **1998**, *31*, 18−25.
(43) Kirmaier, K.; Holten, D. *The Photosynthetic Bacterial Reaction Center—Structure and Dynamics*; Plenum: New York, 1988.